Rosenau, M., Oncken, O. (2009): Fore-arc deformation controls frequency-size distribution of megathrust earthquakes in subduction zones. - Journal of Geophysical Research, 114, B10311

DOI: 10.1029/2009JB006359.

Forearc deformation controls frequency-size distribution of megathrust earthquakes in subduction zones

Matthias Rosenau[1] and Onno Oncken[1]

Abstract

Seismotectonic deformation in subduction zones seems to follow rather simple spatiotemporal patterns with forearc basins overlying the areas of large slip during quasi-periodic megathrust earthquakes. To study the possible coupling between long-term deformation and earthquake behavior we use compressive granular wedges overlying a rate- and state-dependent frictional interface as analogue models of subduction zone forearcs overlying a seismogenic megathrust. For different seismogenic zone geometries, we analyze deformation time-series with respect to the accumulation of permanent strain and frequency-size distributions of episodic slip events equivalent to great (M > 8) earthquakes. We observe that permanent deformation in the wedges localizes at the periphery of unstable slip at depth over tens of simulated seismic cycles. For updip limited seismogenic zone models, this leads to structural wedge segmentation characterized by an elastic domain overlying the zone of unstable basal slip. Along with the evolution of segmentation the frequency-size distributions of episodic slip events develop from more random, Gutenberg-Richter-like events (*b-value* ~ 0.6) towards more periodic, characteristic events (*b-value* < 0.1). Corresponding coefficients of variation of recurrence intervals decrease from C_v ~ 0.6 in deforming wedges to C_v ~ 0.3 in segmented wedges. From the experiments we thus infer a positive feedback between forearc tectonics and megathrust seismogenesis which brings the system from a stochastic to a more deterministic state. Our experimental observations imply that

[1] GeoForschungsZentrum Potsdam (GFZ), Telegrafenberg, D-14473 Potsdam (Germany)

the quasi-periodic recurrence of great subduction earthquakes evident from existing earthquake records is a long-term feature intrinsically related to the seismotectonic segmentation of the forearc wedges.

Index terms: 7223 (Earthquake interaction, forecasting, and prediction), 7240 (Subduction zones), 8020 (Mechanics, theory, and modeling), 8104 (Continental margins: convergent), 8123 (Dynamics: Seismotectonics)

1. Introduction

Most subduction zones show a rather simple spatial and temporal pattern of seismotectonic deformation compared to intra-plate settings. Spatially, subduction zones are characterized by a first-order cross-forearc seismotectonic segmentation into shortened domains near the trench (accretionary prism, splay faults, outer arc high) and the coast overlying largely aseismic parts of the subduction megathrust interface at depth [*Byrne et al.,* 1988; *Ruff and Tichelaar*, 1996]. These shortened domains generally bound a tectonically stable shelf region including forearc basins which correlate with the areas of large slip during megathrust earthquakes [e.g., *Mogi*, 1969; *Nishenko and McCann*, 1979, *von Huene and Klaeschen*, 1999; *Song and Simons*, 2003; *Wells et al.,* 2003; *Nicol and Beavan,* 2003]. Temporally, great (M > 8) subduction megathrust earthquakes often show a quasi-periodic pattern of recurrence [e.g., *Kelleher et al.,* 1973; *McCann et al.,* 1979; *Shimazaki and Nakata*, 1980; *Nishenko and Buland*, 1987; *Nishenko,* 1991; *Goldfinger et al.,* 2003; *Bookhagen et al.,* 2006; *Cisternas et al.,* 2005; *Sykes and Menke*, 2006; *Sieh et al.,* 2008; *Bondevik*, 2008, and references therein]. This implies that the megathrust earthquake process in subduction zones is more deterministic (time-dependent) compared to intraplate settings. The latter are generally characterized by a complex spatiotemporal pattern of seismotectonic deformation suggesting that the underlying process is more stochastic (time-independent) [e.g., *Li et al.,* 2009]. The discrimination between deterministic and stochastic nature of the earthquake process in a specific tectonic setting and constraints on the associated frequency-size distributions has important implications for probabilistic seismic hazard assessment [e.g. *Matthews et al.,* 2002; *Sykes and Menke*, 2006; *Parsons*, 2008; *Kuehn et al.,* 2008]. However, the long recurrence intervals of great subduction megathrust earthquakes and the low resolution of past events generally prevents statistically significant conclusions to be

drawn from historic and paleo-earthquake records [e.g., *Rong et al.,* 2003; *McCaffrey*, 2008; *Li et al.,* 2009].

To better understand the coupling between forearc tectonics and great megathrust earthquakes, we simulate time-series of seismotectic deformation with an experimental approach. We use compressive granular wedges featuring a stick-slip mechanism of basal sliding (analogue earthquake cycles) controlled by rate- and state-dependent friction as quasi-two-dimensional models of subduction zones. The models are scaled for strength, gravitation, inertia and elasticity. Simulating a large number (> 100) of seismic cycles allows us to analyze the frequency-size statistics of simulated great (M > 8) megathrust earthquakes and study possible feedback mechanisms between long-term deformation and earthquake behavior.

2. Experimental Setup

The experimental setup used in this study is a modification of conventional quasi-two-dimensional sandbox setups [e.g., *Lohrmann et al.*, 2003] monitored from one side with an industrial strain analysis system (particle image velocimetry, PIV). The experimental method has been described in detail by *Rosenau et al.* [2009]. Here we recall the basics of the approach and report modifications specific to the present study.

2.1. Model scaling

The experimental device consists of a glass-sided box (1000 mm long x 500 mm high x 100 mm wide) with a basal conveyer plate on top of which a granular compressive wedge (subduction forearc model) is set up and compressed against a rigid backwall (Figure 1). Dynamic similarity between the model and nature has been achieved with respect to strength, gravitation, inertia and

elasticity by keeping the following set of dimensionless quantities constant during down-scaling the natural prototype:

- Strength ratio τ = ratio between gravitation and strength
- Friction coefficient μ = pressure-dependency of strength
- Friction rate parameter *a-b* = rate- and state-dependency of frictional strength
- Froude Number *Fr* = ratio between inertia and gravitation
- Cauchy Number *Ca* = ratio between inertia and compressibility

Conservation of these dimensionless quantities dictates the experimental conditions and analogue material properties (Table 1) in terms of scaling factors [*Hubbert,* 1937]. The scaling factors (ratio between quantities in model and nature) for length, mass, and (interseismic) time in the presented model setups are $5 \cdot 10^{-6}$, $4 \cdot 10^{-17}$ and $1.3 \cdot 10^{-10}$, respectively. Consequently 1 cm in the model corresponds to 2 km in nature and 1 second is equivalent to about 250 years. The convergence rate in the experiments has been equivalent to 50 mm/a in nature. Each experimental run took 1000 seconds or 250.000 years if scaled to nature. In this study we treat the subduction forearc lithosphere as purely brittle, so viscoelastic effects of the lower crust and mantle are neglected. Other processes important in morphotectonics and seismogenesis (erosion, sedimentation, isostacy, pore fluids) are also neglected here for the sake of simplicity.

2.2. Material properties

The compressible wedges used in this study are made of flavored rice, refined sugar and rubber pellets Intergranular slip in rice and sugar both obey a rate- and state-dependent friction law and

has been used to simulate the seismic and aseismic slip behavior of the subduction megathrust. More specifically, slip along surfaces in rice is velocity weakening (i.e. the friction coefficient decreases with increasing slip rate) with a friction rate parameter a-b of typically -0.015 (Table 1) as determined by ring shear tests [*Rosenau et al*., 2009]. At laboratory normal loads (< 10 kPa) this results in unstable sliding accompanied by cyclic loss and regain of strength (stick-slip) similar to the seismic cycle deformation [e.g. *Scholz*, 1998]. Noticeably, even at very low normal stresses (10 Pa equivalent to less than a millimeter model overburden), sliding in rice is unstable [*Rosenau et al*., 2009] suggesting that no conditionally stable regime [*Scholz*, 1998] exists in the models. Sugar has a lower friction coefficient than rice (~0.7 vs. ~0.8) and shows velocity strengthening behavior at laboratory normal loads with a-b ~ +0.015 [*Rosenau et al*., 2009]. This results in stable sliding similar to the aseismic deformation of sediments present along shallow parts of the megathrust [e.g. *Saffer and Marone*, 2003] and hydrated mantle rocks at greater depth [e.g. *Reinen et al*., 1994]. Rubber (EPDM) pellets has been mixed with rice and sugar to achieve properly scaled elasticity of the model wedges (bulk modulus k = 0.1 MPa or about 60 GPa in nature).

2.3. Model Configuration

The quasi-two-dimensional subduction zone models presented here represent a 200-km-long section of brittle (elastoplastic) forearc lithosphere (Figure 1). The 10° dipping megathrust includes a seismogenic zone (SZ) of unstable stick-slip deformation (velocity weakening behavior, a-b < 0) limited up- and downdip by aseismic zones of stable sliding (velocity strengthening behavior, a-b > 0) similar to subduction zones like Chile and Alaska [e.g., *Oleskevich et al.,* 1999]. As a result of rate- and state-dependent frictional properties of the material used the wedges feature transient basal strength profiles shown in Figure 1: High slip

rates (> 1 mm/s) during episodic (< 0.1 s duration) slip events (analogue earthquakes) cause a strength drop within the SZ coincident with a strength increase outside of it. During the stick ("interseismic") period the strength of the SZ recovers to strengths larger than those of the stable sliding zones.

We present an experimental series including three model configurations (Figure 1) and analyze the accumulation of permanent deformation and frequency-size distribution of analogue earthquakes equivalent to M > 8 events in nature. The only parameter varied in the models is the position of the updip limit of the SZ. The downdip limit has been kept constant at 70 cm from the wedge tip (140 km from the trench in nature). By this we simulate the behavior of subduction zones with variable width and depth of the seismogenic zone: A narrow/deep seismogenic zone model A1 (20 cm wide SZ, SZ updip limit 50 cm from wedge tip), an intermediate wide/intermediate deep seismogenic zone model A2 (40 cm wide SZ, SZ updip limit 30 cm from the wedge tip), and a wide/shallow seismogenic zone model B (70 cm wide SZ, no SZ updip limit).

In models A1 and A2 (hereafter referred to as A-type models) the SZ is limited in the updip direction due to the change in frictional properties from velocity weakening (a-b < 0) to velocity strengthening (a-b > 0) along the megathrust. Therefore ruptures are stalled towards the tip of the wedge by a coseismic strength gradient similar to typical subduction megathrust earthquakes in nature ["seismic front", *Byrne et al.* 1988; *Hyndmann et al*., 1997*; Scholz,* 1998*; Moore and Saffer*, 2001]. In model B (hereafter referred to as B-type model), the frictional properties along the megathrust do not change in the updip direction, i.e. remain in the velocity weakening/unstable slip regime. Assisted by a strong gradient in normal stress at shallow depth

138 controlled by the model geometry this allows ruptures breaking through to the tip of the model
139 wedge simulating trench-breaking earthquakes.

140 **2.4. Monitoring and Deformation Analysis**

141 For strain analysis of the evolving model wedges we have used an optical image acquisition and
142 correlation system (particle image velocimetry, PIV StrainMaster by LaVision, Germany, see
143 *Adam et al.* [2005] and *Rosenau et al.* [2009] for applications in analogue tectonic and earthquake
144 simulation). During an experiment, the locations of particles on one side of the model have been
145 recorded by sequential digital images of a 12-bit monochrome charged-coupled device (CCD)
146 camera acquired at a frequency of 10 Hz. The displacement vector field between successive
147 images has then been determined by cross-correlation of textural differences (i.e. gray values)
148 formed by groups of particles using a Fast Fourier Transform algorithm. The precision of the
149 incremental displacement vector field is better than 5 micrometers. This allows observing
150 episodic slip events corresponding to earthquakes of moment magnitude ~M8 and higher in
151 nature. Based on the vector field local derivative calculations provide the cross-sectional
152 components of the strain tensor. Analogue earthquakes typically occur within a 0.1-second time
153 interval, i.e. are captured by a single PIV image. During visual inspection of the PIV time-series,
154 they are identified by strain rates increased by orders of magnitude.

155 **2.5. Magnitude Scaling**

156 In order to ease comparison of experimental observations with nature, we provide the moment
157 magnitude of the simulated earthquakes along with the laboratory scale observations. Moment
158 magnitude is based on the seismic moment, which includes the lateral (trench-parallel) rupture
159 length not simulated in the current quasi-two-dimensional approach. It is necessary to extrapolate

160 the 2D laboratory observations to 3D. We do this following the procedure described in *Rosenau*
161 *et al.* [2009] which includes basic geometric scaling of slip and trench-normal rupture width
162 (simulated) according to the scaling laws in Table 1 and application of an empirical scaling law
163 of the form:

164

165 $$rupture\ length = 6.5 \cdot 10^{9}\ slip^{1.2} / rupture\ width \quad (1)$$

166

167 to derive a theoretical trench-parallel rupture length. Scaled rupture lengths in the model are
168 limited to 1300 km which corresponds to a mean maximum length of possible earthquakes in
169 subduction zones of the earth [McCaffrey, 2008]. Under this condition, scaled moment
170 magnitudes of the simulated events presented here range from M7.7 to M9.6.

171 **3. Experimental Observations**

172 **3.1. Long-term Evolution of Experimental Subduction Zones**

173 Figures 2 and 3 illustrate the long-term evolution of the experimental subduction zones in terms
174 of permanent (or plastic) strain accumulation: Figure 2 shows the cumulative horizontal
175 shortening E_{xx} (shortening negative) along crustal profiles as well as the finite cross-sectional
176 strain (E_{xx}) pattern. Figure 3 shows the evolution of the long-term rate dE_{xx}/dt of spatially
177 averaged wedge strain (integrating over 20-second-increments in the experiments, which are
178 equivalent to 5-kyr-increments in nature).

179 All model wedges are characterized by decreasing amounts of permanent deformation
180 accumulated over an experimental run as reflected by a narrowing of the cumulative strain curves

in Figure 2 and a decrease in strain rate (Figure 3). Noticeably, the decrease in strain rate is discontinuous in A-type models which are characterized by an order-of-magnitude drop at t = 500 s (Figure 3). The B-type model, in contrast, shows a more continuous decrease in strain rate. In all models shortening within the wedge localizes near the down-dip limit of the SZ in form of a proto-backthrust. In the presence of an updip limit of the seismogenic zone (models type A), shortening also localizes updip of the SZ in the form of proto-thrusts. Shortening is less localized and partitioned into several diffuse shear zones in the B-type model. The finite average shortening of the wedges is about 1 – 2 % in A-type models and about 3 % in the B-type model. This is consistent with about 5 to 15 % of plate convergence taken up by deformation of the overriding plate.

A-type models show a more segmented finite deformation pattern compared to the rather diffuse deformation pattern of model-type B: A-type models are characterized by domain of low permanent deformation (E_{xx} < 1 %) which overlies the SZ (Figure 2). This quasi-elastic domain is limited by plastically shortened domains (E_{xx} ~ 2 – 3 %) at the periphery of the SZ. The one-order-of-magnitude drop in long-term strain rate (Figure 3) at t = 500 s marks the establishment of this structural segmentation after about 60 seismic cycles (Movies 1 and 2). The transition corresponds to ~ 2 % of shortening localized into peripheral shear zones (Figures 2 and 3). In contrast, model type B does not develop a clear segmentation but shows a rather short wavelength finite strain pattern reflecting the accumulation of permanent deformation throughout the wedge and above the SZ (Figure 2 and Movie 3).

3.2. Analogue Earthquake Behavior of Experimental Subduction Zones

The analogue earthquakes generated by the experimental subduction zones are shown in Figure 4 by means of the slip-width scaling and cumulative moment release. As an equivalent to the

seismic moment in nature, we calculated a moment associated with analogue earthquakes as the product of slip, rupture width and bulk modulus. Note that due to the 2D approach only the rupture width and not the length is considered in moment calculation which makes the analogue earthquake moment having the dimension of a force (N). Average slip during analogue earthquakes scale with the rupture width (Figure 4 a) and increases systematically from 29 ± 15 µm in model A1, to 42 ± 23 µm in model A2 and 46 ± 35 µm in model B. The average moments associated with episodic slip events are about 0.58 N ± 0.37 N in model A1, 1.6 N ± 1.1 N in model A2 and 1.9 N ± 2.4 N in model B. The mean recurrence intervals of simulated analogue earthquake sequences are 5 to 6 s. Over an experimental run, the moments consequently accumulate to about 100 N in model A1 and to about 300 N in models A2 and B.

All experimental runs are characterized by an increasing moment release rate from about 100 mN/s to about 500 mN/s (Figure 4 b). Again, A-type models show a rather discontinuous accumulation history including a kink in the cumulative release curve at t = 500 s. After t = 500 s, they are characterized by a very linear trend in Figure 4 b indicating a constant moment release rate following the establishment of peripheral shear zones and structural wedge segmentation at E_{xx} ~ 2 % (Movies 1 and 2). Model B, in contrast, shows a more transient pattern of moment release with long range changes in release rate indicating that episodic slip events cluster while shear zones successively form in the overlying wedge (Figure 4 b and Movie 3).

Analogue Earthquake Statistics

The contrasting strain accumulation and moment release patterns of the A- versus B-type subduction zone models (i.e. segmented versus deforming, constant versus clustered) suggest an intrinsic difference in the analogue earthquake behavior of elastic and plastically deforming wedges. To evaluate this, we statistically analyzed the spatiotemporal pattern of observed

episodic slip events equivalent to M > 8 earthquakes in nature by means of (1) frequency-size distribution fitting (chi-square test) and (2) time-series of the coefficient of variation

A chi-square test provides a measure of the goodness of fit of an observed distribution (here the experimentally generated frequency-size distributions) to theoretical distributions. It tests the null hypothesis that the frequency-size distribution of certain events observed in a subsample is consistent with a particular theoretical distribution. Here we tested the experimental distributions against synthetic normal and exponential distributions (Figure 5). The normal (Gaussian) and exponential distributions are endmember distributions viewed as diagnostic for time-dependent, deterministic and time-independent, stochastic processes, respectively [e.g. *Nishenko and Buland*, 1987; *Matthews et al.,* 2002; *Parsons et al.,* 2008]. The consistency of the fit to these distributions can thus be used as proxies of the probabilistic nature of the underlying process.

To derive a numerical value of distribution consistency, we first calculated the chi-square statistic (χ^2) between the experimentally observed and synthetic distributions. The synthetic distributions were modeled mathematically on the basis of the sample mean and variance given by the experimental distribution. χ^2 is defined as the sum of squared differences between observed (O) and synthetic (S) counts divided by the synthetic counts within each bin of a distribution:

$$\chi^2 = \Sigma_i [(O_i-S_i)^2/S_i] \quad \text{for } i = 1, \ldots, n. \qquad (2)$$

We then compared the chi square statistic with the chi-square distribution by dividing χ^2 by the critical chi-square statistic at a level of significance of 0.05 ($\chi^2_{crit\ 0.05}$). If $\chi^2/\chi^2_{crit\ 0.05} < 1$, the thus

248 normalized chi-square statistic suggests that the probability of the experimental distribution being
249 similar to the synthetic distribution by chance is less than 5 %. In other words: the probability
250 that the experimental and synthetic distributions are the same is 95 %. This is a commonly used
251 threshold criterion for arguing that two distributions are statistically consistent.

252 A second statistical parameter used here is the coefficient of variation (C_v). It is a measure of the
253 dispersion of a given distribution and defined as the ratio of the standard deviation (σ) to the
254 mean (X):

255

256 $$C_v = \sigma / X \qquad (3)$$

257

258 Generally the coefficient of variation scales inversely to the periodicity of the frequency-size
259 distribution. Random, self-similar events are characterized by high $C_v > 1$. Quasi-characteristic
260 events are characterized by low coefficients of variation $C_v < 1$ [e.g. *Kuehn et al.*, 2008, and
261 references therein].

262 Both the distribution fitting/chi-square test and the calculation of the coefficients of variation are
263 based on successive subsamples of the simulated sequences (subsequences) derived by a sliding
264 window technique. Here, we used windows including 49 events shifted by 1 event. Each data
265 point in Figures 6 (results of chi-square test) and 7 (coefficients of variation) thus represents the
266 statistical parameters of a subsequence including the 24 preceding and 24 following events.
267 Analogue earthquake sequences produced by both A-type models share their statistical
268 characteristics. For clarity we here plot only data from the model A2 as it is most comparable to

269 the B-type model in terms of the total amount of moment released during the experiments (see
270 Figure 4 b) and magnitude range of events.

271 Figure 6 shows the results of the distribution fitting/chi-square tests on experimental
272 subsequences of episodic slip events equivalent to great (M > 8) earthquakes in nature with
273 normal versus exponential distributions. Note that a normalized chi-square statistics below one
274 indicates consistency of the observed and theoretical distribution. Because the axes of this plot
275 are equidistant, vertically elongate clusters indicate a better fit to the normal distribution whereas
276 horizontal clusters indicate a better fit to the exponential distribution. In terms of recurrence,
277 normally distributed events indicate a periodic, deterministic behavior whereas exponentially
278 distributed events indicate a random, stochastic recurrence. In terms of size, normally distributed
279 events indicate that they are of a characteristic size whereas exponentially distributed events
280 indicate a self-similar character.

281 Accordingly, episodic slip events generated by models of type A show a preferential fit to the
282 normal distributions both in terms of recurrence and size whereas those of model B show
283 generally a good fit to both the normal and the exponential distributions. This indicates that
284 analogue earthquakes generated by the segmented, more elastic wedges of type A models are
285 periodic and similar in size, i.e. are characteristic events. The hybrid fit of the frequency
286 distributions produced by the B-type model can be attributed to the asymmetry of the
287 distributions, which are generally skewed towards short recurrence intervals (Figure 5). By this,
288 they are more similar to the exponential distribution. This suggests that analogue earthquakes
289 generated by the plastically deforming wedge occur more randomly than those of the segmented,
290 elastic wedges. In terms of size distribution, they are close to a self-similar size distribution, i.e. a
291 Gutenberg-Richter type of earthquake distribution [*Gutenberg and Richter*, 1944].

To visualize the temporal evolution of the frequency-size distributions we plotted the coefficients of variation of subsequences versus time (counted in earthquake cycles) in Figure 7. With respect to the recurrence interval distribution all models are characterized by $C_v < 1$. The C_v of type A models are generally lower than those of the B-type model indicating that they are more periodic. Moreover, they evolve from comparable coefficients of $C_v \sim 0.5 – 0.6$ towards higher periodicity characterized by $C_v \sim 0.3$. The recurrence pattern of the B-type model, in contrast, is less periodic (more random) characterized by systematically higher C_v (~ 0.6) and does not evolve. The size distributions of all models evolve towards lower coefficients of variation indicating that events becomes successively more similar over an experimental run. Type A models generally generate size distributions with a $C_v < 1$ indicating a characteristic earthquake behavior. The B-type model, in contrast, produces earthquakes with magnitudes characterized by $C_v > 1$ indicative of a self-similar, Gutenberg-Richter like size distribution.

The statistical analysis of frequency-size distribution of the experiments suggests that plastically deforming wedges behave in a more random, stochastic way in contrast to the characteristic, deterministic behavior shown by those models which evolved into segmented, elastic wedges.

4. Interpretation

4.1. Relationship Between Analogue Earthquake Slip, Strain localization and Deformation Behavior

In all experimental subduction zones shortening within the wedge localizes at the periphery of the seismogenic zone (SZ) such that wedge structure reflects the distribution of slip behavior (stick-slip vs. stable sliding) at depth. A proto-backthrust evolves at the downdip limit of the SZ in all models. An earlier study [*Rosenau et al.,* 2009] showed that compression here occurs during the

stick-phase due to a downdip increase in thrust motion controlled by the basal strength profile (Figure 1). In the presence of an updip limit of the SZ (models type A), deformation also localizes updip of the SZ in the form of proto-thrusts. Here, the updip change from velocity weakening to velocity strengthening controls the updip increase of friction during episodic slip events (Figure 1). This effectively limits rupture propagation towards the wedge tip (Figure 4 a) and causes compression updip of the SZ during analogue earthquakes. Over multiple events, repeating compression drives strain localization updip of the SZ consistent with predictions of the dynamic Coulomb wedge theory [*Wang and Hu*, 2006].

Noticeably, an updip limit of the SZ seems to be pre-requisite for the models to evolve into segmented wedges with an elastic domain overlying the SZ. The sudden change of deformation behavior from plastically deforming to elastic observed in the A-type models t = 500 s (Figures 2 and 3, Movies 1 and 2) is likely controlled by strain localization into peripheral shear zones. In granular material, strain hardening occurs at low strain levels (< 5 %) and strain weakening after localization [e.g., *Lohrmann et al*., 2003; *Adam et al.*, 2005]. Consistently, the change in deformation behavior occurs at comparable strain values of a few percent (E_{xx} ~ 2 %). This suggests that at t = 500 s , peripheral shear zones accommodated sufficient deformation to enter the strain weakening regime and become weaker than the rest of the wedge material which is still in the strain hardening regime. Being the weakest part of the wedge, any further deformation is partitioned preferentially into them and accumulation of deformation above the SZ is abandoned.

4.2. Feedback of Wedge Deformation Into Analogue Earthquake Behavior

Since wedge shortening takes up part of the plate convergence, accumulation of permanent deformation may feed back into the analogue earthquake process via modifying the basal loading conditions both spatially and temporally. We interpret the strong parallelism of long-term and

337 short-term evolution of the wedges and their analogue earthquake behavior (Figure 3 and 4 b) as
338 indicating that wedge deformation and episodic slip events are coupled processes. More
339 specifically, the structural segmentation evolving in A-type models is directly reflected by the
340 suddenly established constant moment release rate after t = 500 s (Figure 4 b). Moreover,
341 because the part of the wedge overlying the zone of stick-slip deformation behaves elastic, the
342 compressive wedges of type A can be viewed as a simple, deterministic spring-slider system [e.g.
343 *Reid*, 1910]. This is consistent with the observation of a more periodic pattern of analogue
344 earthquakes produced by such wedges (Figures 5 -7). In contrast, ongoing proto-shear zone
345 formation and abandoning in the B-type model may cause a more cyclic hardening and
346 weakening of the wedge. We thus interpret the clustering of episodic slip events shown by the B-
347 type model (Figure 4 b) to reflect the long-range transient changes of the loading condition
348 associated with cyclic wedge hardening-weakening. Moreover, because of ongoing plastic
349 deformation above the SZ, the compressive wedge of type B may behave more like a multiple,
350 stochastic spring-slider system [e.g. *Burridge and Knopoff*, 1967]. This is consistent with the
351 more random, Gutenberg-Richter like analogue earthquake behavior shown by this wedge
352 (Figures 5 - 7).

353 **5. Application to Nature and Discussion**

354 **5.1. Correlation Between Megathrust Earthquake Slip and Long-term Deformation of**
355 **Subduction Forearcs**

356 The experiments demonstrated that the internal structure of a compressive wedge reflects the
357 distribution slip behavior (stick-slip versus stable sliding) along its base. Applied to nature, this
358 observation suggests that a causal relationship exist between morphotectonic segmentation and

great earthquake slip useful for seismic hazard assessment. It implies that the seismogenic zone limits can be mapped using observations related to upper plate structure.

A central point of the seismotectonic evolution of subduction zone as suggested by the models is the localization of deformation at the peripheries of the SZ. Shortening may localize near the trench due to coseismic compression at the updip limit of earthquake ruptures and near the coast due to interseismic compression at the downdip limit of the locking. Similar observations exist in nature. For example, the inversion of global tsunami data [*Mogi*, 1969; *Nishenko and McCann*, 1979] and gravimetric observations [e.g., *Song and Simons*, 2003; *Wells et al.,* 2003] suggest that forearc basins, i.e. tectonically stable settings, generally overly the areas of large slip during megathrust earthquakes. Localization of shortening at the updip limit of the SZ has been quantitatively demonstrated in Alaska [*von Huene and Klaeschen*, 1999]: Here about 70 % of plate convergence is accommodated with the outermost 40-wide Neogene accretionary prism where no slip during the great 1964 earthquake occurred. Very similar to our model prediction, less than the 10 % of plate convergence is accommodated in the shelf region overlying the area of large coseismic slip. Similarly in New Zealand, *Nicol and Beavan* [2003] quantified Neogene cross-forearc shortening to account for 6 – 19 % of plate convergence with localized shortening near the trench and near the coast. Moreover, *Ruff and Tichelaar* [1996] showed that the downdip limit of the SZ globally coincides with the coastline consistent with our model prediction.

Natural, theoretical and experimental observations thus suggest that the morphotectonic segmentation of subduction forearcs is a direct consequence of stress changes associated with megathrust seismic cycles. However, several subduction zone properties and processes not included in the presented model setup may modify the principal pattern of strain localization quantitatively. The long-term average shortening rate of our segmented wedges is in the order of

few tens of nanostrain per year if scaled to nature. This is about one tenth of the short-term, interseismic shortening rates measured geodetically in subduction zones [e.g., *Hyndman and Wang*, 1995] and thus consistent with the ~ 1/10 ratio of long-term versus short-term deformation rates deduced from coastal uplift rates [e.g., *Lajoie*, 1986]. Close to the trench, predictions of our models may be less quantitative. Here, diffuse (ductile) strain resulting from consolidation during accretion of porous, water-rich sediments to the frontal wedge may accommodate up to 10-20 percent of strain prior to localization [e.g., *Morgan et al.,* 1994; *Henry et al*., 2003]. In the model, strain localization at the updip limit of the seismogenic zone and the development of peripheral shear zones occurs at strains about an order of magnitude lower and more likely corresponds to consolidated sediments and crystalline rocks of the brittle crust. Therefore, the finite strain pattern seaward of the seismogenic zone in nature is probably less pronounced in nature, at least with respect to the timescale required to establish it (250.000 years in our simulation). This is particularly the case in settings where large accretionary prisms exist or where the updip limit of the SZ is close to the trench. Depending on the drainage properties of the outer wedge, over pressured fluid and fluid diffusion processes also have important control on the distribution of ductile vs. brittle deformation [*Morgan and Karig*; 1995], the localization and reactivation of faults [e.g., *Bangs et al., 2009*] and time-dependent strength of the outer wedge during the seismic cycle [*Wang and Hu*, 2006]. Moreover, the natural strain pattern may not only reflect stresses changes related to the seismic cycle but also mechanical heterogeneities [*Byrne et al.,* 1988; *Kopp and Kukowsi*, 2003] as well as slab curvature and sedimentation processes [*Fuller et al.*, 2006].

5.2. Feedback of Forearc Tectonics Into Seismogenesis

Our experiments demonstrated that deformation of the wedge overlying the zone of stick-slip deformation causes the frequency-size distributions of episodic slip events to become more random, Gutenberg-Richter like. Vice versa, structurally segmented wedges show a more characteristic episodic slip behavior. We interpreted the different behaviors as due to the similarity of deforming wedges with stochastic, multiple spring-slider systems versus the similarity of segmented wedges with deterministic single spring-slider systems. Applied to nature, this suggests that the earthquake behavior of seismotectonically segmented subduction zone forearcs should be more deterministic (and thus better predictable) than that of more diffusely deforming forearcs.

To visualize the effect of forearc deformation on the frequency-size distributions in nature, Figure 8 shows the simulated cumulative magnitude-frequency curves of great ($M > 8$) earthquakes in deforming versus segmented forearcs as scaled up from episodic slip events of Model B and Model A2 after the establishment of segmentation ($t > 500$ s), respectively. Accordingly, deforming forearcs are predicted to show generally steeper negative slopes of the cumulative distribution in the magnitude range M8 – M9 than segmented forearcs. At the high end of the magnitude range (M9.5), both curves have to drop to zero, because of the finite length of subduction zone earthquakes [*McCaffrey*, 2008], which is set to 1300 km in the scaling law applied here. The corresponding *b-value*, which has been calculated as the negative slope of the linear parts of the curves, is predicted to be about 0.6 in deforming forearcs and smaller than 0.1 in segmented forearcs (Figure 8). The *b-value* predicted for deforming forearcs is at the lower range of *b-values* worldwide, which vary typically between 2/3 and 1 for earthquakes over a wide magnitude range [e.g., *Lay and Wallace*, 1995, Chapter 9]. In deforming forearcs, the shape of the Gutenberg-Richter distribution would thus be expected to depart towards the high end of the magnitude range ($M > 8$) only slightly from the magnitude-frequency trend of smaller ($M < 8$)

events (see inset in Figure 8). In contrast, in segmented forearcs, the magnitude-frequency curve is expected to deviate significantly from the Gutenberg-Richter distribution given by smaller (M < 8) events and show a significant flattening at high magnitudes (M8 – M9.6) indicative of a characteristic behavior of great earthquakes (Figure 8).

Because of the rareness of great earthquakes in nature and the limited resolution of paleoseismological observations, we may however not be able to test our predictions of *b-values* and the shape of the magnitude-frequency distribution at high magnitudes in nature. Based on existing catalogs, it seems more suitable to compare the coefficients of variation (C_v) of great earthquake recurrence in nature and experiment. Our experiments predict that C_v of the recurrence intervals of earthquakes of magnitude M8 and higher in deforming forearcs should be ~ 0.6, and ~ 0.3 in segmented forearcs (Figures 5, 7 and 8). In nature, the coefficients of variation of subduction earthquake recurrence are generally < 0.4 [*Nishenko and Buland*, 1987; *Sykes and Menke*, 2006], at least during historic time and the Holocene. For example, the Holocene tsunami record offshore western North America suggest that great M ~ 9 Cascadia subduction zone earthquakes have occurred about every ~ 600 years during the past 10 kyr [*Goldfinger et al.,* 2003] with a C_v of 0.36 – 0.39 [*Sykes and Menke*, 2006]. Similarly, in southern Chile, in the area of the giant M9.5 1960 Valdivia earthquake, leveling and dating of Holocene strand lines by *Bookhagen et al.* [2006] suggest that great earthquakes have occurred every 180 ± 65 years over the last 3 to 4 kyr, from which a C_v = 0.36 can be calculated. The coefficient of variation of 0.3 – 0.4 indicates a quasi-periodic behavior of natural subduction zone earthquakes and is consistent with our models (Figure 8) considering the segmented nature of forearcs in general (see chapter 5.1).

450 The coefficient of variation is an integral part of time-dependent seismic hazard assessment [e.g.,
451 *Sykes and Mendes*, 2006]. Mean recurrence intervals of segmented forearcs characterized by $C_v \sim$
452 0.3 should be shorter than about 100 years to be useful in long-term earthquake predictions on a
453 decadal scale. Most great subduction earthquakes, however, have recurrence intervals
454 significantly larger than 100 years. Long-term earthquake prediction in subduction settings thus
455 seems to be intrinsically limited by upper plate deformation. Nevertheless, our simulations
456 suggest that it is reasonable to consider a non-random, time-dependent earthquake process for
457 seismic hazard assessment in subduction zones with C_v of great earthquake recurrence
458 significantly smaller than in intraplate settings.

459 **6. Conclusions**

460 We used compressive granular wedges overlying a rate- and state-dependent frictional interface
461 as analogue models of subduction zone forearcs and simulated their seismotectonic evolution.
462 Accordingly, permanent deformation localizes at the peripheries of the zone of unstable slip at
463 depth, interpreted as the megathrust seismogenic zone. Interseismic compression at its downdip
464 limit due to locking drives coastal shortening and uplift. An updip limit of the seismogenic zone
465 localizes shortening near the trench through repeated coseismic compression. Strain localization
466 at the updip limit of the SZ is a prerequisite for the evolution of a seimotectonic segmentation
467 including a forearc basin overlying the area of large megathrust earthquake slip as seen in many
468 subduction zones. Statistical analysis of analogue earthquakes generated by the models
469 demonstrates that segmented forearcs have a more characteristic earthquake behavior compared
470 to the more Gutenberg-Richter like behavior of deforming forearcs. We interpreted the difference
471 in terms of simple versus multiple spring-slider system behavior.

We conclude, that (1) the quasi-periodic recurrence shown by existing earthquake records likely reflects a long-term time-dependent behavior of the earthquake process in subduction zones and that (2) the quasi-periodic behavior is directly related to the structural segmentation of subduction zone forearcs. We thus infer coupling via a positive feedback mechanism between seismogenesis and morphotectonics (seismotectonic feedback) which tends to stabilize the spatiotemporal patterns of seismotectonic deformation in subduction zones towards a characteristic earthquake behavior. This seismotectonic feedback brings the system to a more deterministic stage of evolution. Although long-term earthquake prediction might be intrinsically limited by forearc deformation, our results support the incorporation of time-dependent probability models for seismic hazard assessment in subduction zones. Moreover it is suggested that the limits of the seismogenic zone can be mapped using observations related to upper plate structure.

Appendix

Notation

a-b	friction rate parameter.		M	dimension of mass.
Ca	Cauchy Number.		M	moment magnitude.
C_v	Coefficient of variation.		ρ	density, kg/m³.
χ^2	Chi-square statistic.		σ	*standard deviation.*
E_{xx}	horizontal strain.		t	characteristic time, s.
Fr	Froude Number.		τ	strength ratio.
g	gravitational acceleration, m/s².		T	dimension of time.
l	characteristic length, m.		μ	friction coefficient.
L	dimension of length.		v	characteristic velocity, m/s.
k	bulk modulus, Pa.		X	mean.

Acknowledgements

We thank Günter Tauscher, Frank Neumann and Thomas Ziegenhagen for engineering and technical assistance; and Tom Parsons, an anonymous reviewer, the associate editor, and Patrick Taylor for constructive reviews of the manuscript and helpful comments. Research has been funded by the German Ministry of Education and Research (BMBF) and the German Research Foundation (DFG), grant 03G0594 (to M.R.) and GFZ Potsdam. This is publication no. GEOTECH-1221 of the R&D-Program GEOTECHNOLOGIEN.

513 **References**

514 Adam, J., et al. (2005), Shear localisation and strain distribution during tectonic faulting - New
515 insights from granular-flow experiments and high-resolution optical image correlation
516 techniques, *Journal of Structural Geology*, *27*, 183-301, doi:10.1016/j.jsg.2004.08.008.
517 Bangs, N.L.B., et al. (2009), Broad, weak regions of the Nankai Megathrust and implications for
518 shallow coseismic slip, *Earth and Planetary Science Letters*, doi:10.1016/j.epsl.2009.04.026.
519 Bondevik, S. (2008), The sands of tsunami time, Nature, 455, 1183-1184.
520 Bookhagen, B., Echtler, H. P., Melnick, D., Strecker, M. R., and J. Q. G. Spencer (2006), Using
521 uplifted Holocene beach berms for paleoseismic analysis on the Santa Maria Island, south-
522 central Chile, *Geophysical Research Letters, 33*, doi:10.1029/2006GL026734.
523 Burridge, R. and L. Knopoff (1967), Model and theoretical seismicity, *Bull. Seismol. Soc. Am.,*
524 *57,* 341-367.
525 Byrne, D. E., Davis, D. M., and L. R. Sykes (1988), Loci and maximum size of thrust
526 earthquakes and the mechanics of the shallow region of subduction zones, *Tectonics, 7,* 833-
527 857.
528 Cisternas, M., et al. (2005): Predecessors of the giant 1960 Chile earthquake, *Nature, 437*, 404-
529 407, doi:10.1038/nature03943.
530 Fuller, C. W., et al. (2006), Formation of forearc basins and their influence on subduction zone
531 earthquakes, *Geology*, *34*, 65-68, doi: 10.1130/G21828.1.
532 Goldfinger, C., et al. (2003), Holocene earthquake records from the Cascadia subduction zone
533 and northern San Andreas fault based on precise dating of offshore turbidites, *Annu. Rev.*
534 *Earth Planet. Sci., 31*, 555-577, doi: 10.1146/annurev.earth.31.100901.141246.
535 Gutenberg, B., and C. F. Richter (1944), Frequency of earthquakes in California, *Bull. Seismol.*
536 *Soc. Am*., 34, 164– 176.

Henry, P. et al. (2003), Anisotropy of electrical conductivity record of initial strain at the toe of the Nankai accretionary wedge, *Journal of Geophysical Research, 108*, doi:10.1029/2002JB002287..

Hubbert, M. K. (1937), Theory of scale models as applied to the study of geological structures, *Geological Society of America Bulletin, 48,* 1459–1520.

Hyndmann, R. D., Yamano, M., and D. A. Oleskevich (1997): The seismogenic zone of subduction trhust faults*, The Island Arc, 6*, 244-260.

Hyndman, R. D., and K. Wang (1995): The rupture zone of Cascadia great earthquakes from current deformation and the thermal regime, *Journal of Geophysical Research, 100,* paper number: 95JB01970.

Kelleher, J., Sykes, L., and J. Oliver (1973), Possible criteria for predicting earthquake locations and their application to major plate boundaries of the Pacific and Carribean, *Journal of Geophysical Research, 78,* 2547-2585.

Kuehn, N.M., Hainzl, S., and F. Scherbaum (2008), Non-Poissonian earthquake occurence in coupled stress release models and ist effect on seismic hazard, *Geophys. J. Int*., doi.: 10.1111/j.1365-246X.2008.03835.x

Kopp, H. and N. Kukowski (2003), Backstop geometry and accretionary mechanics of the Sundamargin, *Tectonics, 22,,* doi:10.1029/2002TC001420.

Lajoie, K. R. (1986), Coastal Tectonics, in *Active Tectonics, Studies in Geophysics,* pp. 95-124, , National Academic Press, Washington, D. C., USA.

Lay, T. and T. C. Wallace (1995), *Modern Global Seismology*, *International Geophysics Series, 58*, 521 pp., Academic Press Limited, London, UK.

Li, Q., Liu, M., and S. Stein (2009), Spatiotemporal Complexity of Continental Intraplate Seismicity: Insights from Geodynamic Modeling and Implications for Seismic Hazard

561 Estimation, *Bull. Seismol. Soc. Am., 99*, 1, 52-60, doi: 10.1785/0120080005.

562 Lohrmann, J., et al. (2003), The impact of analogueue material properties on the geometry,
563 kinematics, and dynamics of convergent sand wedges, *Journal of Structural Geology*, *25*,
564 1691-1711.

565 Matthews, M.V., Ellsworth, W.L., and P.A. Reasenberg (2002), A Brownian Model for Recurrent
566 Earthquakes, *Bull. Seismol. Soc. Am., 92,* 2233-2250.

567 Mogi, K. (1969), Relationship between the occurrence of great earthquakes and tectonic
568 structures, *Bull. Earthquake Res. Inst. Univ. Tokyo, 47*, 429-451.

569 McCaffrey, R. (2008), Global frequency of magnitude 9 earthquakes, *Geology, 36,* 263-266, doi:
570 10.1130/G24402A.1.

571 McCann, W. R., S. P. Nishenko, L. R. Sykes, and J. Krause (1979), Seismic gaps and plate
572 tectonics: Seismic potential for major boundaries, *Pure Appl. Geophys., 117*, 1082–1147.

573 Moore, J. C., and D. Saffer (2001): Updip limit of the seismogenic zone beneath the accretionary
574 prism of southwest Japan: An effect of diagenetic to low-grade metamorphic processes and
575 increasing effective stress, *Geology, 29*, 183-186.

576 Morgan, J.K., and D.E. Karig (1995), Kinematics and a balanced and restored cross-section
577 across the toe of the eastern Nankai accretionary prism, *Journal of Structural Geology, 17,* 31-
578 45.

579 Morgan, J.K., Karig, D.E., and A. Maniatty (1994), The estimation of diffuse strains in the toe of
580 the western Nankai accretionary prism: A kinematic solution *Journal of Geophysical*
581 *Research, 99,* 7019-7032, doi: 0148-0227/94/93JB-03367505.00.

582 Nicol, A. and J. Beavon (2003), Shortening of an overriding plate and its implications for slip on
583 a subduction thrust, central Hikurangi Margins, New Zealand, *Tectonics, 6,* doi:
584 10.1029/2003TC001521.

585 Nishenko, S.P. (1991), Circum-Pacific seismic potential: 1989-1999, *Pure and Apllied*
586 *Geophysics, 135,* 169-259.

587 Nishenko, S. and W. McCann (1979), Large thrust earthquakes and tsunamis: Implications for the
588 development of forearc basins, *Journal of Geophysical Research, 84,* 573-584, paper number:
589 0148-0227/79/028 B.

590 Nishenko, S.P. and R. Buland (1987), A generic recurrence interval distribution for earthquake
591 forecasting, *Bull. Seismol. Soc. Am., 77*, 13-82-1399.

592 Oleskevich, D. A., et al. (1999), The updip and downdip limits to great subduction earthquakes:
593 Thermal and structural models of Cascadia, south Alaska, SW Japan, and Chile, *Journal of*
594 *Geophysical Research*, *104*, 14965-14991, paper number 1999JB900060.
595 Parsons, T. (2008), Earthquake recurrence on the south Hayward fault is most consistent with a
596 time dependent, renewal process, *Geophys. Res. Let., 35*, doi:10.1029/2008GL035887.
597 Reid, H.F. (1910), On mass-movements in tectonic earthquakes, in *The California earthquake of*
598 *April 18, 1906: Report of the state earthquake investigation commission*, Carnegie Institute of
599 Washington, D.C., USA.
600 Reinen, L. A., et al. (1994), The frictional behavior of lizardite and antigorite serpentinites:
601 experiments, constitutive models, and implications for natural faults, *Pure and Apllied*
602 *Geophysics*, *143*, 317-358, paper number: 0033-4553/94/030317.

603 Rong, Y. F., et al. (2003), Seismic gaps and earthquakes, *Journal of Geophysical Research, 108*,
604 14. doi:10.1029/2002JB002334.
605 Rosenau, M., J. Lohrmann, and O. Oncken (2009), Shocks in a box: An analogue model of
606 subduction earthquake cycles with application to seismotectonic forearc evolution, *Journal of*
607 *Geophysical Research*, doi:10.1029/2008JB005665, in press.
608 Ruff, J. R., and B. W. Tichelaar (1996), What controls the seismogenic plate interface in
609 subduction zones? in *Subduction: Top to Bottom, Geophysical Monograph 96,* edited by G. E.
610 Bebout et al., pp. 105-111, *AGU, USA*.
611 Saffer, D. M., and C. Marone (2003), Comparison of smectite- and illite-rich gouge frictional
612 properties: Application to the updip limit of the seismogenic zone along subduction
613 megathrusts, *Earth and Planetary Science Letters 215*, 219-235, doi: 10.1016/S0012-
614 821X(03)00424-2.
615 Satake, K., and B.F. Atwater (2007), Long-Term Perspectives on Giant Earthquakes and
616 Tsunamis at Subduction Zones, *Annu. Rev. Earth Planet. Sci., 35*, 349–74, doi:
617 10.1146/annurev.earth.35.031306.140302.
618 Scholz, C. H. (1998), Earthquakes and friction laws, *Nature*, *391*, 37-42.
619 Sieh, K. et al. (2008), Earthquake supercycles inferred from sea-level changes recorded in the
620 corals of West Sumatra*, Science, 322*, 1674-1678, doi: 10.1126/science.1163589.
621 Shimazaki, K., and T. Nakata (1980), Time-predictable recurrence model for large earthquakes,
622 *Geophysical Research Letters*, *7*, 279–282.
623 Song, T. R. A., and M. Simons (2003), Large trench-parallel gravity variations predict
624 seismogenic behavior in subduction zones, *Science*, *301*, 630-633.
625 von Huene, R., and D. Klaeschen (1999), Opposing gradients of permanent strain in the aseismic
626 zone and elastic strain across the seismogenic zone of the Kodiak shelf and slope, Alaska,

627 *Tectonics*, *18*, 248-262, paper number: 1998TC900022.

628 Wang, K., and Y. Hu (2006), Accretionary prisms in subduction earthquake cycles: The theory of

629 dynamic Coulomb wedge, *Journal of Geophysical Research, 111,* doi:

630 10.1029/2005JB004094.

631 Wells, R. E., et al. (2003), Basin-centered asperities in great subduction zone earthquakes: A link

632 between slip, subsidence, and subduction erosion? *Journal of Geophysical Research, 108*, doi:

633 10.1029/2002JB002072.

634

635 **Captions**

636 **Figure 1.** Analogue model configurations. Compressive wedges include variably wide stick-slip
637 zones (seismogenic zones, SZ). A-type models have an updip limit of the SZ, the B-type model
638 not. As a result of rate- and state-dependent frictional properties of the material used the wedges
639 feature transient basal strength profiles: High slip rates during analogue earthquakes (eq) cause a
640 strength drop within the SZ contemporary with a strength increase outside of it. During the stick
641 (interseismic locking) period the strength of the SZ recovers to strengths slightly larger than those
642 of the stable sliding (aseismic) zones outside. See notations for abbreviations used.

643 **Table 1.** Material properties, experimental conditions, scaling and similarity. See notations for
644 abbreviations used.

645 **Figure 2.** Spatiotemporal pattern of long-term permanent deformation within the experimental
646 subduction zones: Cumulative horizontal strain E_{xx} (shortening negative, 100-second-increments
647 corresponding to 25-kyr-increments in nature) along profiles through the wedges and finite
648 patterns of E_{xx}. Note that accumulation of permanent strain ceases over an experimental run and
649 localizes at the peripheries of the seismogenic zones (SZ) causing wedge segmentation. Only in
650 A-type models (updip limited SZ), the SZ is finally overlain by a tectonically stable domain of
651 low permanent strain.

652 **Figure 3.** Long-term strain rate evolution of the experimental subduction zones. Shown is
653 average wedge horizontal strain E_{xx} (shortening negative) during 20-second-intervals
654 (corresponding to 5-kyr-increments). Note the drop in strain rate of A-type models at time t =
655 500 s, which corresponds to about 2 % of wedge shortening (Figure 2), indicating the change

656 from internally deforming wedges to segmented, elastic wedges. A laboratory strain rate of 0.01
657 % per 20 seconds correspond to about 20 nanostrain per year in nature. See text for discussion.

658 **Figure 4**. Episodic slip moment release pattern of experimental subduction zones: (a) Scaling of
659 slip with rupture width of episodic slip events (corresponding magnitudes scaled to nature and
660 seismogenic zone (SZ) updip limits indicated); (b) cumulative moment release curves. Note the
661 constant release of A-type models after time ~ t = 500 s (corresponding to ~ 2 % of permanent
662 strain accumulated in the wedge) versus the transient rate changes of B-type model.

663 **Figure 5.** Examples of frequency-size distribution**s** of episodic slip events equivalent to great (M
664 > 8) earthquakes in nature. Coefficients of variation (C_v) of recurrence intervals and size and
665 upper and lower cut-off magnitudes extrapolated to nature indicated. The distributions shown as
666 insets are the best-fit synthetic distributions.

667 **Figure 6.** Results of frequency-size distribution fitting/chi-square test. Shown are the normalized
668 chi-square statistics ($\chi^2/\chi^2_{\text{crit }0.05}$) of recurrence (left column) and size distributions (right column)
669 of episodic slip events equivalent to great (M > 8) earthquakes in nature. Each data point gives
670 the consistency between a subsample distribution composed of a 49 events and the normal versus
671 exponential distributions. $\chi^2/\chi^2_{\text{crit }0.05} < 1$ suggests statistical significant consistency of the
672 observed and theoretical distributions. Vertical and horizontal elongation of clusters indicates a
673 preferential fit to normal and exponential distribution, respectively. Note that A-type models
674 (only model A2 shown here for clarity) produce more normally distributed events versus more
675 exponentially distributed events of the B-type model. This is consistent with more periodic,
676 characteristic (deterministic) events of segmented, elastic wedges versus more random, self-
677 similar (stochastic) events of deforming wedges. See text for discussion.

678 **Figure 7.** Evolution of the frequency-size distribution of episodic slip events equivalent to great
679 (M > 8) earthquakes in nature. Shown is the temporal evolution of the coefficient of variation
680 (C_v) over multiple simulated seismic cycles ($C_v > 1$: random, self-similar events; $C_v < 1$: quasi-
681 characteristic events). Note that A-type models (only model A2 shown here for clarity) show
682 generally a lower variability and evolve towards a more characteristic behavior.

683 **Figure 8.** Predicted earthquake behavior of deforming versus segmented forearcs. Plot shows
684 cumulative magnitude-frequency distributions of great (M > 8) earthquakes scaled from the
685 model B for deforming forearcs and from model A2 (post-500-second) for the segmented
686 forearcs. *b-values*, which has been calculated as the negative slope of the linear parts of the
687 curves, and coefficients of variation (C_v) of earthquake recurrence indicated. At the high end of
688 the magnitude range (M9.5), both curves have to drop to zero, because of the finite length of
689 subduction zone earthquakes.

690 **Auxiliary material (Dynamic content)** ***See also "readme" File***

691 **Movie 1.** Structural evolution of model A1. Color code illustrates cumulative horizontal strain E_{xx}
692 (shortening negative) accumulated during 20-second-increments (corresponding to 5-kyr-
693 increments in nature).

694 **Movie 2.** Structural evolution of model A2. Color code illustrates cumulative horizontal strain E_{xx}
695 (shortening negative) accumulated during 20-second-increments (corresponding to 5-kyr-
696 increments in nature).

697 **Movie 3.** Structural evolution of model B. Color code illustrates cumulative horizontal strain E_{xx}
698 (shortening negative) accumulated during 20-second-increments (corresponding to 5-kyr-
699 increments in nature).

Figure 1

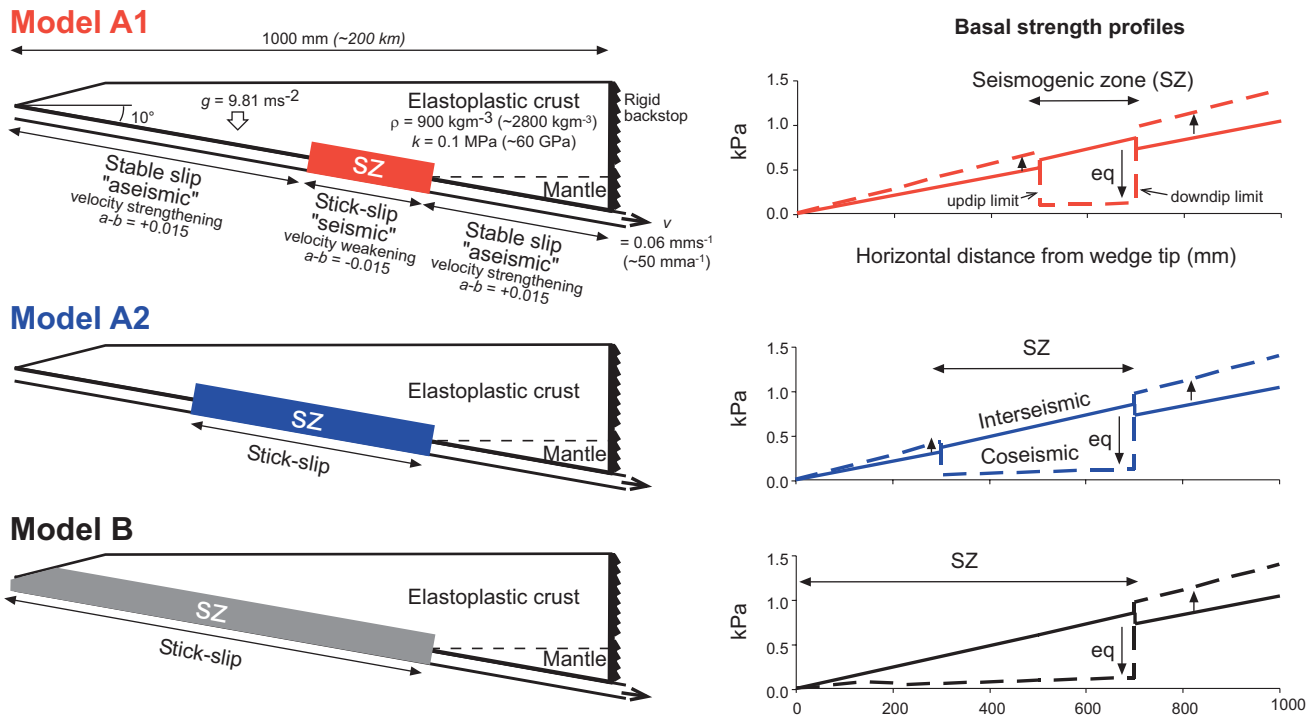

Figure 1. Analogue model configurations. Compressive wedges include variably wide stick-slip zones (seismogenic zones, SZ). A-type models have an updip limit of the SZ, the B-type model not. As a result of rate- and state-dependent frictional properties of the material used the wedges feature transient basal strength profiles: High slip rates during analogue earthquakes (eq) cause a strength drop within the SZ contemporary with a strength increase outside of it. During the stick (interseismic locking) period the strength of the SZ recovers to strengths slightly larger than those of the stable sliding (aseismic) zones outside. See notations for abbreviations used.

Table 1. Analogue Model Parameters, Material Properties, Experimental Conditions, Scaling, and Similarity[a]

	Parameters				Similarity						
	Quantity	Symbol	Dimension {M,L,T}	Unit	Model		Nature		Dimesionless number	Scaling factor	
Model parameters	Length	l	L	[m]	1	mm	200	m		5×10^{-6}	Geometric similarity
	Time (interseismic)	t	T	[s]	1	s	250	a		1.3×10^{-10}	Kinematic similarity
	Time (coseismic)	t	T	[s]	0.1	s	45	s		2.2×10^{-3}	
	Convergence velocity	v	L/T	[m/s]	0.06	mm/s	50	mm/a		3.9×10^{4}	
	Rupture velocity	v	L/T	[m/s]	5	m/s	2.2	km/s		2.2×10^{-3}	
	Acceleration	g	L/T^2	[m/s^2]	9.81	m/s²	9.81	m/s²	$Fr = v(gl)^{-0.5}$	1	Dynamic similarity
Material properties	Friction coefficient	μ	1		0.7 / 0.8		0.7 / 0.8		μ	1	
	Friction rate parameter	a-b	1		±0.015		±0.015		a-b	1	
	Bulk modulus	k	M/LT^2	[Pa]	0.1	MPa	62	GPa	$Ca = \rho v^2/\mu$	1.6×10^{-6}	
	Density	ρ	M/L^3	[kg/m^3]	900	kg/m^3	2800	kg/m^3		3.2×10^{-1}	

[a]See notation in Appendix for the abbreviations used.

Figure 2

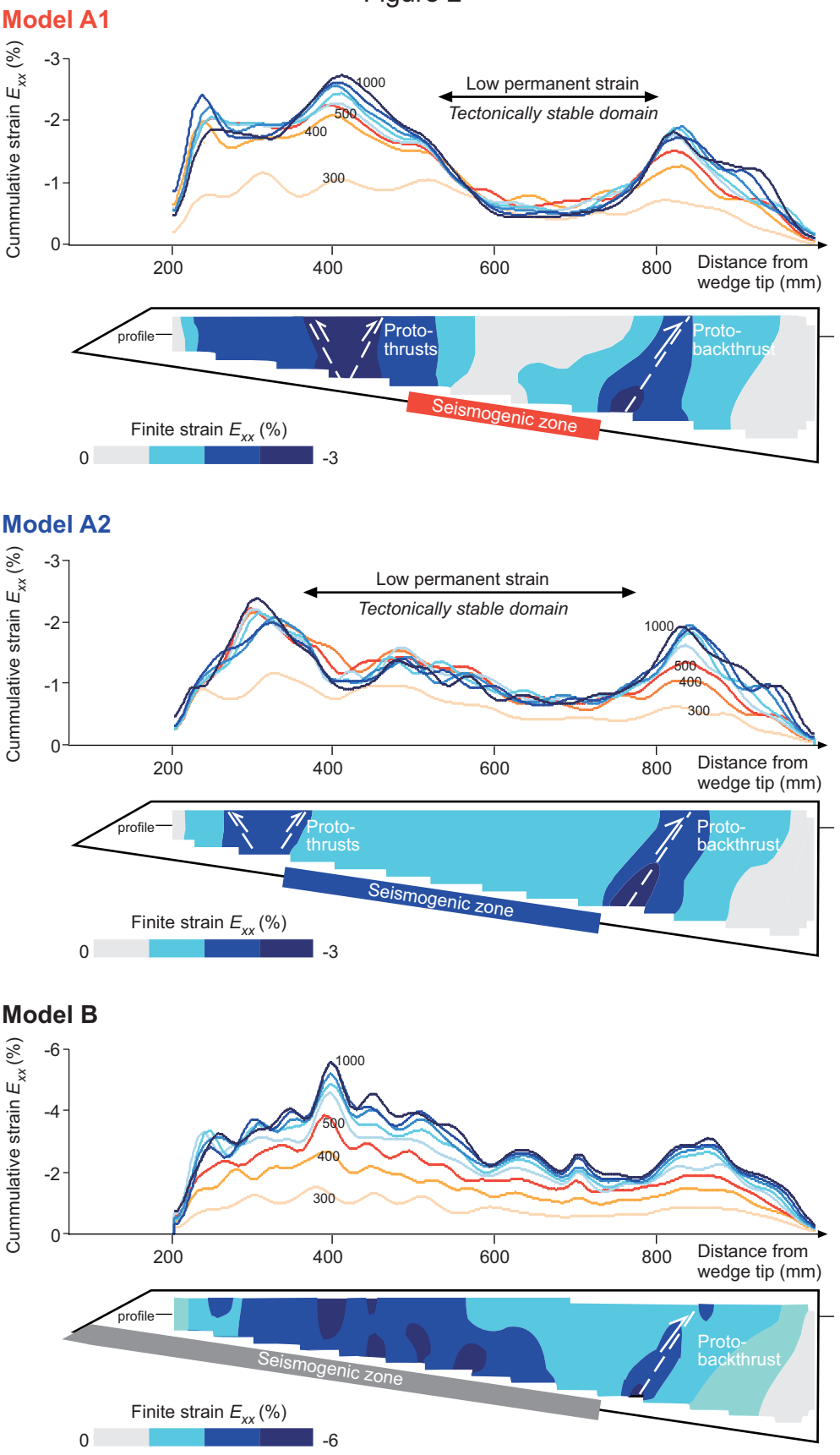

Figure 2. Spatiotemporal pattern of long-term permanent deformation within the experimental subduction zones: Cumulative horizontal strain E_{xx} (shortening negative, 100-second-increments corresponding to 25-kyr-increments in nature) along profiles through the wedges and finite patterns of E_{xx}. Note that accumulation of permanent strain ceases over an experimental run and localizes at the peripheries of the seismogenic zones (SZ) causing wedge segmentation. Only in A-type models (updip limited SZ), the SZ is finally overlain by a tectonically stable domain of low permanent strain.

Figure 3

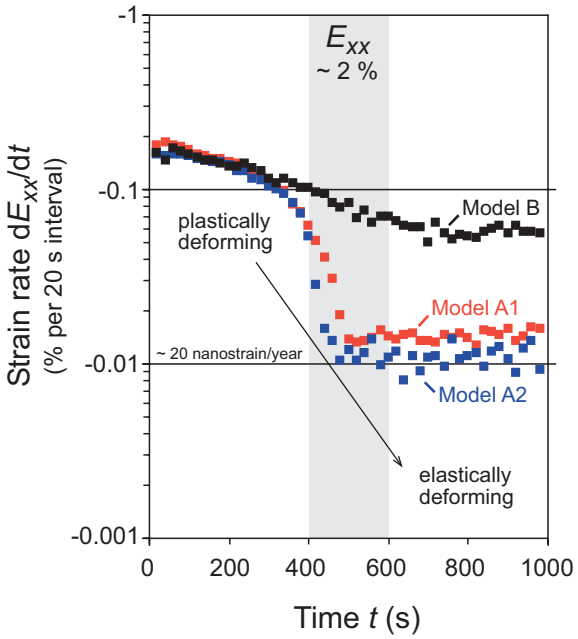

Figure 3. Long-term strain rate evolution of the experimental subduction zones. Shown is average wedge horizontal strain E_{xx} (shortening negative) during 20-second-intervals (corresponding to 5-kyr-increments). Note the drop in strain rate of A-type models at time t = 500 s, which corresponds to about 2 % of wedge shortening (Figure 2), indicating the change from internally deforming wedges to segmented, elastic wedges. A laboratory strain rate of 0.01 % per 20 seconds correspond to about 20 nanostrain per year in nature. See text for discussion.

Figure 4

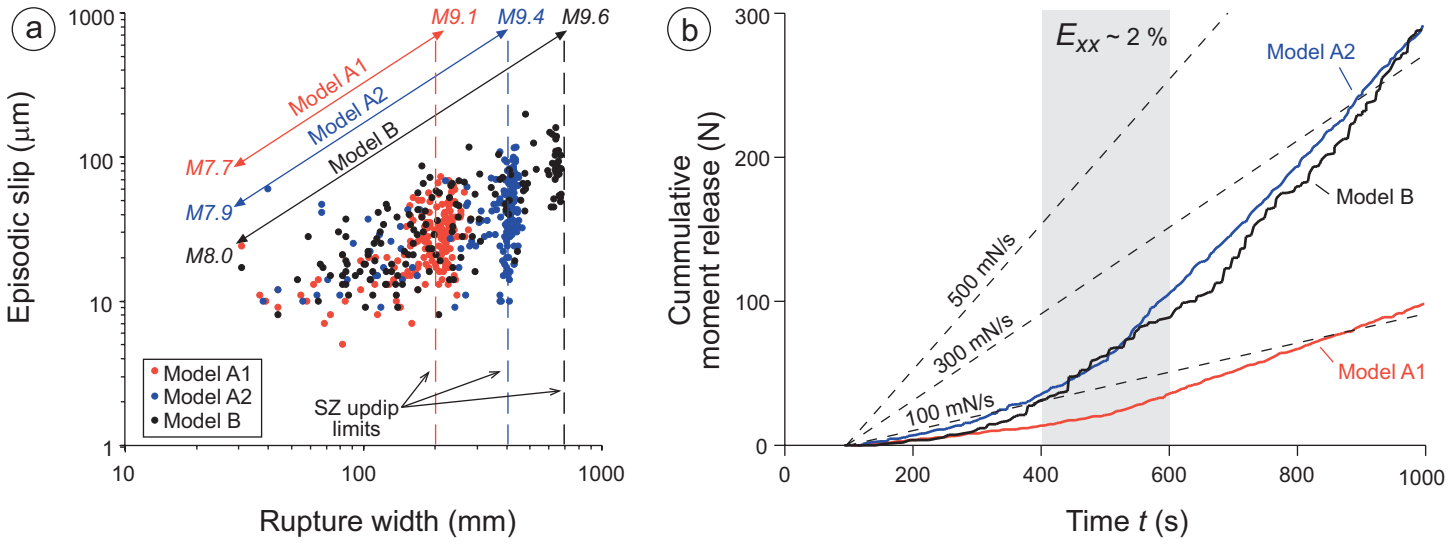

Figure 4. Episodic slip moment release pattern of experimental subduction zones: (a) Scaling of slip with rupture width of episodic slip events (corresponding magnitudes scaled to nature and seismogenic zone (SZ) updip limits indicated); (b) cumulative moment release curves. Note the constant release of A-type models after time ~ t = 500 s (corresponding to ~ 2 % of permanent strain accumulated in the wedge) versus the transient rate changes of B-type model.

Figure 5

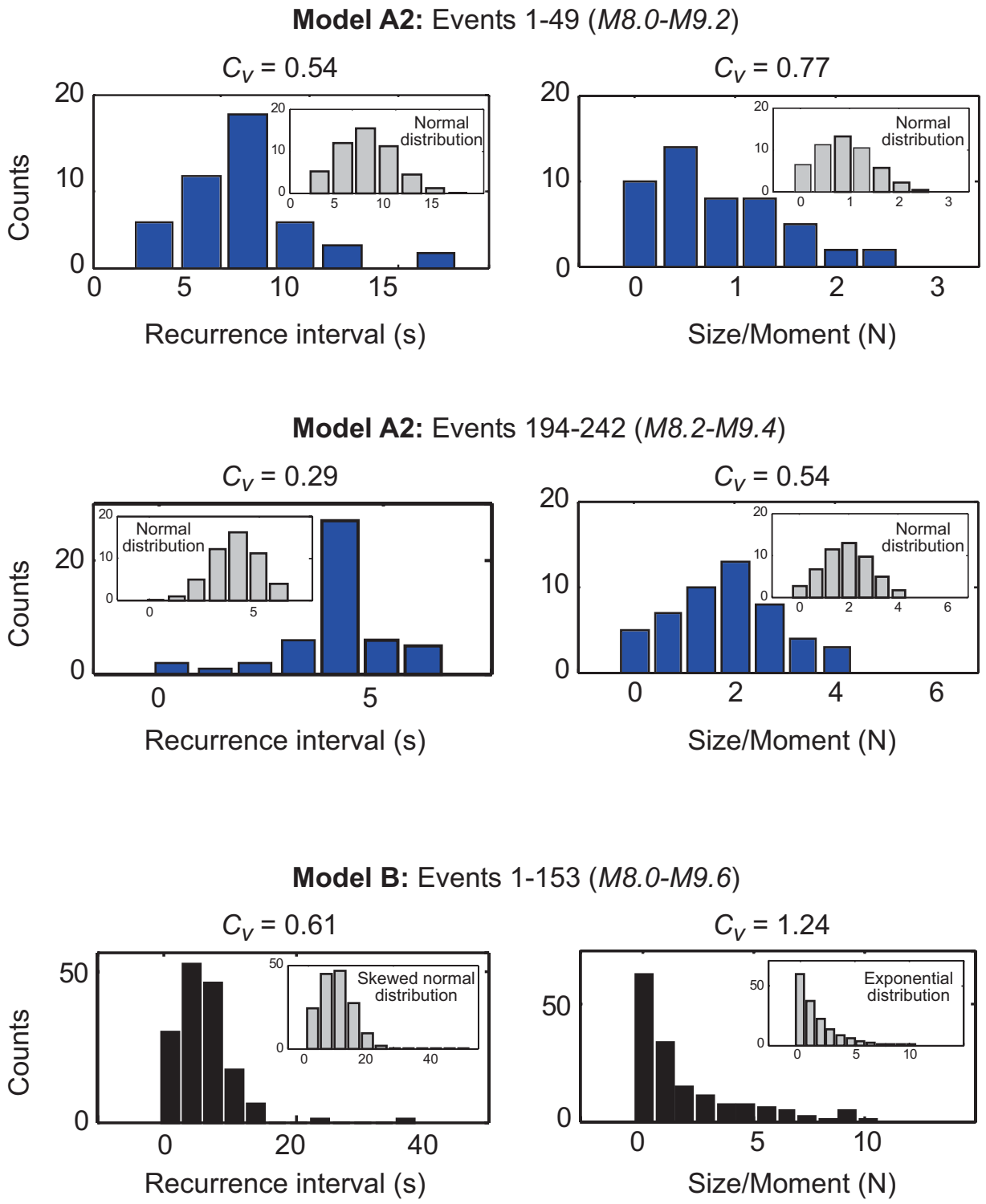

Figure 5. Examples of frequency-size distribution**s** of episodic slip events equivalent to great (M > 8) earthquakes in nature. Coefficients of variation (C_v) of recurrence intervals and size and upper and lower cut-off magnitudes extrapolated to nature indicated. The distributions shown as insets are the best-fit synthetic distributions.

Figure 6

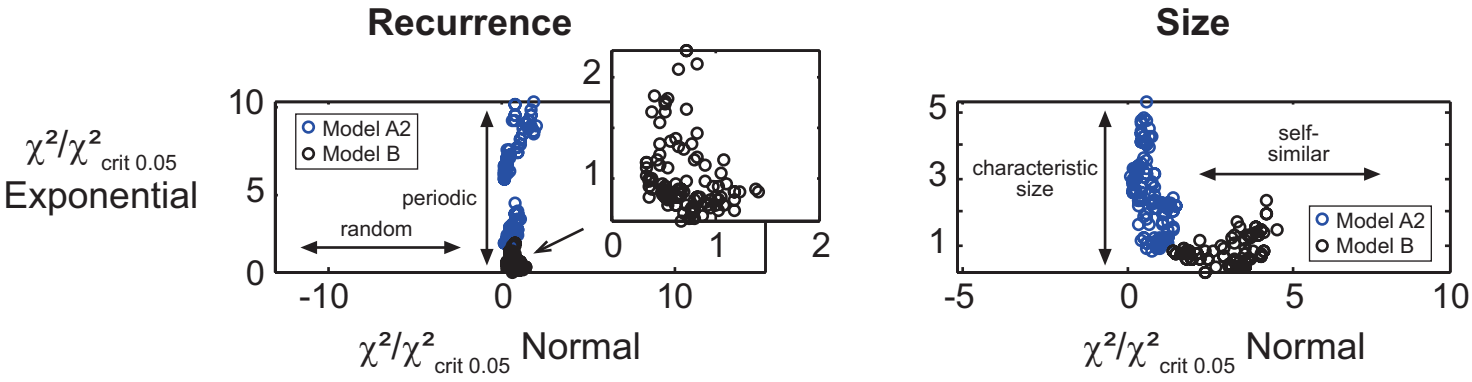

Figure 6. Results of frequency-size distribution fitting/chi-square test. Shown are the normalized chi-square statistics ($\chi^2/\chi^2_{crit\ 0.05}$) of recurrence (left column) and size distributions (right column) of of episodic slip events equivalent to great (M > 8) earthquakes in nature. Each data point gives the consistency between a subsample distribution composed of a 49 events and the normal versus exponential distributions. $\chi^2/\chi^2_{crit\ 0.05} < 1$ suggests statistical significant consistency of the observed and theoretical distributions. Vertical and horizontal elongation of clusters indicates a preferential fit to normal and exponential distribution, respectively. Note that A-type models (only model A2 shown here for clarity) produce more normally distributed events versus more exponentially distributed events of the B-type model. This is consistent with more periodic, characteristic (deterministic) events of segmented, elastic wedges versus more random, self-similar (stochastic) events of deforming wedges. See text for discussion.

Figure 7

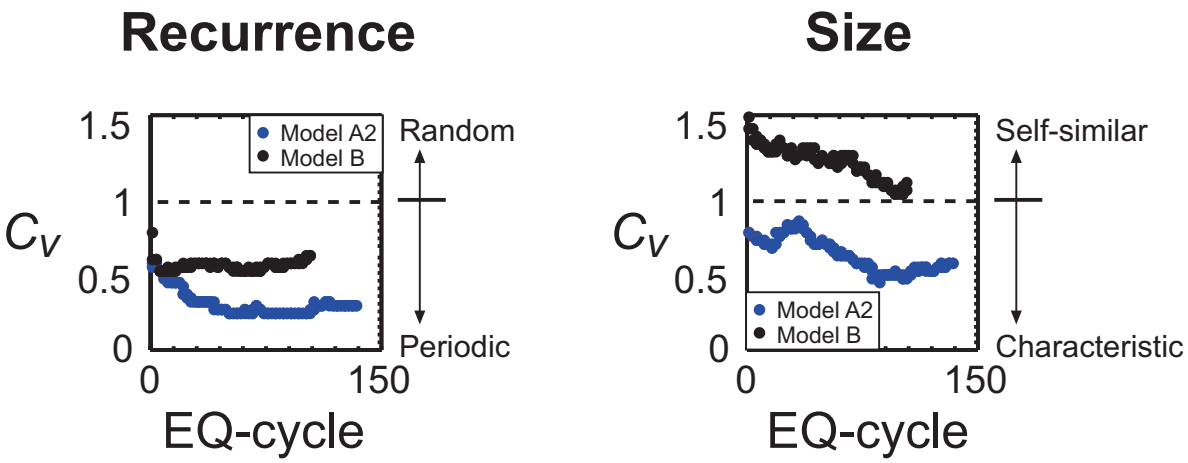

Figure 7. Evolution of the frequency-size distribution of episodic slip events equivalent to great (M > 8) earthquakes in nature. Shown is the temporal evolution of the coefficient of variation (C_v) over multiple simulated seismic cycles ($C_v > 1$: random, self-similar events; $C_v < 1$: quasi-characteristic events). Note that A-type models (only model A2 shown here for clarity) show generally a lower variability and evolve towards a more characteristic behavior.

Figure 8

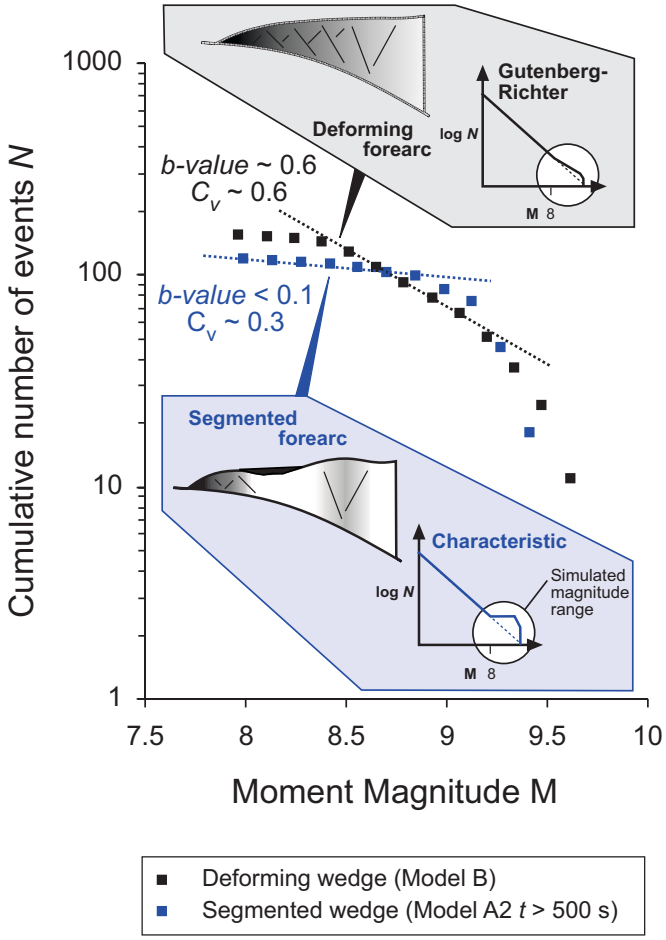

Figure 8. Predicted earthquake behavior of deforming versus segmented forearcs. Plot shows cumulative magnitude-frequency distributions of great (M > 8) earthquakes scaled from the model B for deforming forearcs and from model A2 (post-500-second) for the segmented forearcs. *b-values*, which has been calculated as the negative slope of the linear parts of the curves, and coefficients of variation (C_v) of earthquake recurrence indicated. At the high end of the magnitude range (M9.5), both curves have to drop to zero, because of the finite length of subduction zone earthquakes.